THE JOURNAL OF BIOLOGICAL CHEMISTRY VOL. 284, NO. 24, pp. 16343–16353, June 12, 2009

Structural and Biophysical Characterization of the Proteins Interacting with the Herpes Simplex Virus 1 Origin of Replication[S]

Received for publication, August 8, 2008, and in revised form, March 17, 2009 Published, JBC Papers in Press, March 27, 2009, DOI 10.1074/jbc.M806134200

Ioannis Manolaridis[‡§1,2], Eleni Mumtsidu[‡1,3], Peter Konarev[‡¶4], Alexander M. Makhov[‖], Stephen W. Fullerton[‡2], Andrea Sinz[**], Stefan Kalkhof[**], John E. McGeehan[§], Peter D. Cary[§], Jack D. Griffith[‖], Dmitri Svergun[‡¶4], Geoff G. Kneale[§], and Paul A. Tucker[‡5]

From [‡]European Molecular Biology Laboratory, Hamburg Outstation, D-22603 Hamburg, Germany, [§]Biophysics Laboratories, Institute of Biomedical and Biomolecular Sciences, University of Portsmouth, Portsmouth PO1 2DT, United Kingdom, [‖]Lineberger Comprehensive Cancer Center, University of North Carolina, Chapel Hill, North Carolina 27599-7295, [**]Institute of Pharmacy, Martin Luther University Halle-Wittenberg, D-06120 Halle, Germany, and [¶]Institute of Crystallography, Russian Academy of Sciences, Leninsky pr. 59, 117333 Moscow, Russia

The C terminus of the herpes simplex virus type 1 origin-binding protein, UL9ct, interacts directly with the viral single-stranded DNA-binding protein ICP8. We show that a 60-amino acid C-terminal deletion mutant of ICP8 (ICP8ΔC) also binds very strongly to UL9ct. Using small angle x-ray scattering, the low resolution solution structures of UL9ct alone, in complex with ICP8ΔC, and in complex with a 15-mer double-stranded DNA containing Box I of the origin of replication are described. Size exclusion chromatography, analytical ultracentrifugation, and electrophoretic mobility shift assays, backed up by isothermal titration calorimetry measurements, are used to show that the stoichiometry of the UL9ct-dsDNA$_{15\text{-mer}}$ complex is 2:1 at micromolar protein concentrations. The reaction occurs in two steps with initial binding of UL9ct to DNA ($K_d \sim 6$ nM) followed by a second binding event ($K_d \sim 0.8$ nM). It is also shown that the stoichiometry of the ternary UL9ct-ICP8ΔC-dsDNA$_{15\text{-mer}}$ complex is 2:1:1, at the concentrations used in the different assays. Electron microscopy indicates that the complex assembled on the extended origin, oriS, rather than Box I alone, is much larger. The results are consistent with a simple model whereby a conformational switch of the UL9 DNA-binding domain upon binding to Box I allows the recruitment of a UL9-ICP8 complex by interaction between the UL9 DNA-binding domains.

The initiation of DNA replication for most double-stranded DNA (dsDNA)[6] viral genomes begins with the recognition of the origin by specific origin-binding proteins. The herpes simplex virus type 1 (HSV-1) genome encodes seven proteins required for origin-dependent DNA replication. These are the DNA polymerase (UL30) and its accessory protein (UL42), a heterotrimeric helicase-primase complex (UL5, UL8, and UL52), the single-stranded DNA-binding protein (ICP8 or UL29), and the origin-binding protein (UL9) (reviewed in Ref. 1). HSV-1 contains three functional origins, oriL and two copies of oriS. OriS, which is about 80 bp in length, consists of three UL9 recognition sites, in Boxes I, II, and III, which are arranged in two overlapping palindromes (2). Box I and Box III are part of an evolutionarily conserved palindrome that forms a stable hairpin in single-stranded DNA, which may be important in the origin rearrangement (3) during initiation of replication. Box I and II are separated by an AT-rich spacer sequence, which varies in length and nucleotide composition between the different members of the α-herpesvirus subfamily (2, 4–6).

UL9 is a homodimer in solution, and EM studies, with UL9 bound to oriS, indicate the existence of a dimer or pair of dimers assembled on oriS (7). Several reports indicate that UL9 can physically interact not only with ICP8 (8) but also with other members of the HSV-1 replication complex, including UL8 (9) and UL42 (10). Thus UL9 functions as a docking protein to recruit these essential replication proteins to the viral origins. ICP8 stimulates the helicase activity of UL9 (11, 12) and binds to its C-terminal 27-aa residues (13). In the presence of ICP8, UL9 will open dsDNA containing Box I, leading to a conformational change in the origin, thus facilitating unwinding (14–16). As stated above, the changes in DNA conformation in the complete oriS may be more complex (3). Recently, it has been suggested that single-stranded oriS folds into a unique and evolutionarily conserved conformation, oriS*, which is stably bound by UL9. oriS* contains a hairpin formed by complementary base pairing between Box I and Box III in oriS (17). UL9, in the presence of the single-stranded DNA-binding protein ICP8, can convert an 80-bp double-stranded minimal oriS fragment to oriS* and form a UL9-oriS* complex. The formation of a UL9-oriS* complex requires ATP hydrolysis (18). Therefore,

[S] The on-line version of this article (available at http://www.jbc.org) contains supplemental text, Figs. S1–S8, and Tables S1 and S2.

[1] Both authors contributed equally to this work.

[2] Supported by contract LSHG-CT-2004-S11960 from the European Union Integrated Project "VIZIER."

[3] Present address: PerkinElmer Cellular Technologies, Schnackenburgallee 114, D-22525 Hamburg, Germany.

[4] Supported by Contract 011934 from the European Union Design Study "SAXIER."

[5] To whom correspondence should be addressed: European Molecular Biology Laboratory, Hamburg Outstation, Notkestrasse 85, D-22603 Hamburg, Germany. Tel.: 49-40-89902-129; Fax: 49-40-89902-149; E-mail: tucker@embl-hamburg.de.

[6] The abbreviations used are: dsDNA, double-stranded DNA; ssDNA, single-stranded DNA; EMSA, electrophoretic mobility shift assay; aa, amino acid; HSV-1, herpes simplex virus type 1; SAXS, small angle x-ray scattering; ITC, isothermal titration calorimetry.

the UL9-oriS* complex may serve as an assembly site for the herpesvirus replisome. Macao *et al.* (3) proposed a model in which full-length UL9 would be required to adopt a different conformation when binding to oriS or oriS*. The implication is that UL9 partially unwinds and introduces a hairpin into the origin of replication and that the formation of oriS* is aided, in some way, by ICP8 and requires ATP hydrolysis. Macao *et al.* (3) suggest that the length of the single-stranded tail of the probe DNA determines the stoichiometry of the UL9-DNA complex. oriS may bind two molecules of UL9, whereas oriS* may only bind one because the hairpin formation prevents the second interaction.

Photo-cross-linking studies have shown that, although the UL9 protein binds Box I as a dimer, only one of the two monomers contacts Box I, suggesting that the C terminus of UL9 undergoes a conformational change upon binding to Box I (19). The results reported here are consistent with this observation. To date there is no three-dimensional structural information available on the full-length UL9 or either of the functionally characterized (helicase and DNA binding) domains. The ability to adopt different conformations and a tendency to proteolytic degradation may be responsible for this. It has been shown that UL9 binds with very high specificity to the Box I through its DNA-binding domain, consisting of the C-terminal 317 aa (UL9ct) (20, 21). Although the importance of the binding between UL9ct and oriS for the viral life cycle is well established, the mechanism behind this interaction still remains unclear. Even though UL9ct exists as a monomer in solution, uncertainty remains as to whether one or two molecules bind to a single Box I recognition sequence. Some reports have suggested that one UL9ct molecule binds to a single copy of the sequence (22–24), whereas others have proposed that UL9ct forms a dimer when bound to DNA (25, 26). This apparent difference may well result from the different protein concentrations used in different assays/experiments, which in turn highlights the difficulty of translating *in vitro* equilibrium experiments into cellular nonequilibrium situations.

A few years ago, the crystal structure of a 60-residue C-terminal deletion mutant of ICP8 (ICP8ΔC) was determined to 3 Å resolution (Protein Data Bank code 1URJ (27)). The structure of ICP8ΔC consists of a large N-terminal domain (aa 9–1038) and a smaller entirely helical C-terminal domain (aa 1049–1120) connected to the N-terminal domain by a disordered linker (aa 1038–1049) spanning around 18 Å in the crystal structure. ICP8 preferentially binds ssDNA over dsDNA in a nonsequence-specific and cooperative manner (28). ICP8 is a zinc metalloprotein containing one zinc atom per molecule, which is coordinated by three cysteines (Cys-499, Cys-502, and Cys-510) and a histidine (His-512) (27).

In this study, we show that the 60-amino acid C-terminal deletion of ICP8 (ICP8ΔC) binds strongly to UL9ct. We present three low resolution structures in solution using small angle x-ray scattering as follows: that of the UL9ct alone, in complex with ICP8ΔC, and in complex with a 15-mer dsDNA ($dsDNA_{15\text{-}mer}$) containing the Box I sequence. Using these data and a variety of biophysical techniques, we demonstrate that the stoichiometries of the UL9ct-$dsDNA_{15\text{-}mer}$ and UL9ct-ICP8ΔC-$dsDNA_{15\text{-}mer}$ complexes are 2:1 and 2:1:1, respectively, at the micromolar protein concentrations used in this study. Using EM we visualize the assembly of the ICP8ΔC-UL9ct complex on oriS and estimate the size of the complex.

EXPERIMENTAL PROCEDURES

Materials—Insect-cell culture media and reagents were obtained from Invitrogen, and the oligonucleotides were from MWG and Eurogentec. *Escherichia coli* BL21(DE3)pLysS cells and the pET-23b plasmid were obtained from Novagen.

Expression and Purification of Native and Mutant UL9ct Proteins—The UL9ct clone was a kind gift of Dr. N. Stow (MRC Virology Unit, Glasgow, Scotland, UK) (29). A single colony of *E. coli* strain BL21(DE3)pLysS transformed with the appropriate plasmid was inoculated overnight at 30 °C in 5 ml of LB medium supplemented with 50 μg ml^{-1} ampicillin and 34 μg ml^{-1} chloramphenicol. One ml of culture was used to inoculate 1 liter of LB medium supplemented with the same antibiotics. For the native protein, after growing at 30 °C to $A_{600} = 0.8$, the culture was rapidly cooled to 15 °C, and expression was induced with 1 mM isopropyl β-D-thiogalactopyranoside. Harvesting took place after 12–14 h of expression at 15 °C. Finally, the cells were harvested by centrifugation at 11,500 × *g*, and the pellets were stored at −20 °C until required.

A pellet from 1 liter of cells was resuspended in 30 ml of buffer-L1 (20 mM HEPES-NaOH, pH 8.0, 100 mM NaCl, 0.5 mM EDTA, 1 mM dithiothreitol, and 10% (v/v) glycerol). The cells were sonicated, and the supernatant was separated from the cell debris by centrifugation at 64,000 × *g* (Beckman SA-300 rotor) for 1 h at 4 °C. The protein was purified over an SP-Sepharose (1 ml) column followed by a heparin (1 ml) column. In each case, once the base line had been reached, a linear gradient from 100 to 1000 mM NaCl in buffer-L1 was used to elute the protein. A final purification step using size exclusion chromatography was carried out using a Superdex-75 (10/30) column. The UL9ct concentration was estimated from the theoretical molar extinction coefficient at 280 nm (38,305 M^{-1} cm^{-1}).

Insect Cell Expression and Purification of ICP8ΔC—expreSF+ insect cells (Protein Sciences Corp.) were maintained in Sf900II medium supplemented with 100 units ml^{-1} penicillin/streptomycin (Invitrogen) and grown in 2.5-liter suspension flasks (Fernbach) to a cell density of 4 × 10^6 cells ml^{-1}. Cells were diluted 1:2 prior to infection with the recombinant baculovirus at a multiplicity of infection of 5. Sixty five to 70 h after infection, cells were harvested, washed twice in cold phosphate-buffered saline, and frozen at −80 °C.

The insect cell pellets from 300 ml of insect cell culture were resuspended in 50 ml of lysis buffer-L2 (50 mM Tris-HCl, pH 8.0, 150 mM NaCl, 1 μg ml^{-1} DNase I, and 4 tablets of protease inhibitor mixture (Roche Applied Science)) and homogenized by sonication. The lysed cells were cleared by centrifugation at 64,000 × *g* for 1 h in a Beckman SA-300 rotor. The protein solution was applied to a 5-ml nickel-chelating column followed by a gel filtration column (Superdex-200) using an Äkta purifier (Amersham Biosciences) equipped with the three-dimensional kit. The His_6-tagged protein constructs were purified following a standard three-dimensional Äkta purifier protocol with a combined low imidazole (5 mM imidazole) and a high salt (500 mM NaCl) washing step. The proteins were eluted

from the nickel-chelating column with buffer-L2 + 500 mM imidazole. The final gel filtration and storage buffer was buffer-GF (50 mM Tris-HCl, pH 8.0, 150 mM NaCl, and 5% (v/v) glycerol).

Formation and Purification of the ICP8ΔC-UL9ct Complex—The UL9ct-ICP8ΔC complex was purified using one of two strategies as follows: 1) either by mixing the separately purified proteins together in the appropriate molar ratio and running the mixture through a gel filtration (Superdex-200) column, or 2) by mixing the corresponding cell lysates together and following a three-dimensional kit protocol (Amersham Biosciences) with a nickel-chelating column followed by size exclusion chromatography. The nature of the complex did not depend on the manner of preparation (note that only ICP8ΔC is His_6-tagged).

Formation and Purification of the 15-mer dsDNA Template and the Binary and Ternary Complexes—Two 15-base-long oligonucleotides were purchased to form the $dsDNA_{15\text{-mer}}$, the F15-mer 5′-gcgttcgcacttcgt-3′ and the R15-mer 5′-acgaagtgcgaacgc-3′. Equimolar amounts of the complementary oligonucleotides were mixed, heated to 90 °C for 20 min in annealing buffer-A (10 mM Tris-HCl, pH 8.0, 10 mM $MgCl_2$, and 150 mM NaCl), and cooled slowly to 4 °C overnight to achieve complete annealing. The duplex DNA was separated from un-annealed ssDNA using size exclusion chromatography (Superdex-75). The DNA concentration was calculated based on the reduced molar extinction coefficient (230,000 $M^{-1}cm^{-1}$) calculated by summing the nucleoside extinction coefficients at 260 nm and subtracting 18% to correct for the hypochromic effect in the duplex. In the case of hexachlorofluorescein-labeled $dsDNA_{15\text{-mer}}$ (hex-$dsDNA_{15\text{-mer}}$), the contribution of the fluorescent tag, at 260 nm, was also taken into account (~10%).

To test complex formation using EMSA, different molar ratios of the $dsDNA_{15\text{-mer}}$ template and the pre-purified UL9ct (see above) were mixed and incubated for 30 min at 4 °C in buffer-GF. The ternary complex was investigated in a similar manner. For the SAXS experiments on the UL9ct-$dsDNA_{15\text{-mer}}$ complex, a 2:1 molar ratio was used, followed by a polishing step using a gel filtration column (Superdex-200) to separate the protein-DNA complex from any unbound dsDNA.

Isothermal Titration Calorimetry—UL9ct and the DNA duplex were prepared and purified as described above. During this experiment, buffer-A1 (20 mM HEPES-NaOH, pH 8.0, 100 mM NaCl, 10% (v/v) glycerol) was used, instead of annealing buffer-A. The 1-ml fractions, corresponding to dsDNA, were stored at −20 °C. ITC measurements were carried out in duplicate on a MicroCal VP-ITC instrument at 25 °C. DNA (463 μM) was injected into 1.8 ml of buffer-A1 containing UL9ct (15.8 μM). The volume of DNA per injection was 2.5 μl. The UL9ct and DNA concentrations were determined as described above. The kcal/mol per injection was fitted by a two-step reaction using the Origin software (MicroCal), after subtracting −0.9 kcal/mol, corresponding to the approximate average of the control experiment, namely titrating buffer without DNA into the UL9ct solution.

Analytical Size Exclusion Chromatography of the Binary and Ternary Complexes—Hex-$dsDNA_{15\text{-mer}}$ (final concentration 3 μM) was incubated with ICP8ΔC (1:1 molar ratio) and with ICP8ΔC and UL9ct (1:1:1 molar ratio). In this case, the buffer used was 20 mM HEPES-NaOH, pH 8.0, 100 mM NaCl, 1 mM EDTA, 10% (v/v) glycerol, and 1 mM dithiothreitol. The elution was performed on a Superose 6 HR 10/30 column. A second experiment was performed on the native UL9ct-$dsDNA_{15\text{-mer}}$ complex at two protein:DNA ratios (*i.e.* 1:1 and 2:1) and a final DNA concentration of 5 μM. This analysis was performed using a Superose 12 10/300 GL column, run at 1 ml min^{-1} and 4 °C on an Äkta purifier system. The column was equilibrated with 2 column volumes of buffer-GF. The nucleoprotein complexes and free DNA were loaded onto the column in 250-μl aliquots, following its calibration with high molecular weight markers (Amersham Biosciences).

Sedimentation Velocity of the UL9ct-DNA Complex—Native UL9ct was mixed with $dsDNA_{15\text{-mer}}$ at 4:1 monomer protein to DNA ratio at 2.4 μM final DNA concentration. Complex (400 μl) and buffer (425 μl) were loaded into a standard double-sector EPON cell with quartz glass window assemblies of 12-mm optical path length. The cell was subsequently loaded into an AN50-Ti analytical rotor and transferred to the centrifuge, where it was left to equilibrate at 4 °C. The rotor was accelerated to 42,000 rpm, and scans were taken every 10 min at 262 nm until complete depletion of sample at the meniscus was observed. The data produced were analyzed using the *c*(*s*) program present in the UltraScan 7.1 software package. The partial specific volume (V_P) used for the analysis of the complex data (0.71 ml g^{-1}) was calculated based on Equation 1 that takes into account the individual V_P values of UL9ct (0.73 ml g^{-1}, calculated by SEDNTERP (30)) and DNA (0.55 ml g^{-1} (31)), and the stoichiometric ratio of the two (2:1 protein monomers to DNA (32)).

$$V_{P(PnD)} = \frac{(nM_P V_{P(P)} + M_D V_{P(D)})}{(nM_P + M_D)} \quad \text{(Eq. 1)}$$

where $V_{P(PnD)}$ is the partial specific volume of the nucleoprotein complex; *n* is the number of protein monomers; $V_{P(P)}$ is the partial specific volume of UL9ct; M_P is the molecular weight of UL9ct; $V_{P(D)}$ is the partial specific volume of DNA; and M_D is the molecular weight of the DNA used.

EMSA—Different molar ratios of protein in buffer-GF were mixed with equal volumes of the $dsDNA_{15\text{-mer}}$, containing the Box I UL9 recognition site (annealed F15-mer 5′-gcgttcgcacttcgt-3′ and R15-mer 5′-acgaagtgcgaacgc-3′). The binding reactions, typically 30–40 μl, were left to equilibrate at 4 °C for 30 min before loading onto a 1.0% TBE-agarose gel in 0.5× TBE buffer. Following electrophoresis at 8 V cm^{-1} for 3 h, DNA was visualized with ethidium bromide, and the proteins were visualized with Coomassie Brilliant Blue staining.

Electron Microscopy on the Complexes of UL9ct-ICP8ΔC with the Herpes Simplex Virus Type 1 Origin Containing DNA (oriS)—In a typical reaction (50 μl) pGEM822 plasmid DNA (33) or the 822-bp HSV-1 BamHI fragment containing oriS isolated from pGEM822 was mixed with the 1:1 UL9ct-ICP8ΔC complex in binding buffer (20 mM Tris-HCl, pH 7.5, 50 mM NaCl, 5 mM $MgCl_2$, and 1 mM dithiothreitol) to give final concentrations of 3 μg ml^{-1} of DNA (150–250 ng) and 45 μg ml^{-1} of protein (2.25 μg). The mixture was incubated for 1 h at 37 °C, then fixed with 0.6% glutaraldehyde (final concentration) for 5 min, and

chromatographed over 2-ml columns of 10% agarose beads (Agarose Bead Technology, Colna, Portugal) to remove free protein and fixatives. The fractions containing DNA-protein complexes were collected, mixed with spermidine (2.5 mM final concentration), adsorbed onto glow-charged thin carbon foils, dehydrated through a water-ethanol series, and rotary shadow-cast with tungsten (34). The samples were examined using a Tecnai 12 instrument at 40 kV or Philips CM12 instrument at 80 kV. Images were recorded on SO-163 film (Eastman-Kodak Co.) at magnifications of 35,000, 45,000, or 60,000, and the images were scanned with an Imacon 848 film scanner (Hasselblad A/S, Gothenburg, Sweden). The contrast was optimized, and images were arranged using Adobe Photoshop software. The molecular mass of UL9ct-ICP8ΔC complexes bound to oriS was evaluated as described previously (35). In brief, 1:1 complexes of UL9ct-ICP8ΔC were formed on a linear fragment containing oriS, and following fixation and just prior to mounting, apoferritin (Sigma) (443 kDa) was added. In micrographs, the projected area of several apoferritin particles was determined, averaged, and compared with the projected area of the oriS-DNA complex. Conversion to volume ratios was carried out on the assumption that the apoferritin and oriS-DNA complexes were spherical, and this was converted to a mass ratio. The mass of the duplex DNA within the complex was excluded from consideration based on the assumption that it does not significantly affect the net volume of the complex.

Small Angle X-ray Scattering Measurements—The synchrotron radiation x-ray scattering data were collected on the X33 beamline of the EMBL on the storage ring DORIS III (DESY, Hamburg, Germany) (36). Solutions of UL9ct protein and its complexes with ICP8ΔC protein (UL9ct/ICP8ΔC) and $dsDNA_{15\text{-mer}}$ (UL9ct/DNA) were measured at 15 °C in the solute concentration range between 0.8 and 1.5 mg ml^{-1} in buffer-GF. The data were recorded using a MAR345 two-dimensional image plate detector at a sample-detector distance of 2.7 m and a wavelength of $\lambda = 1.5$ Å, covering the range of momentum transfer $0.12 < s < 4.5$ nm^{-1} ($s = 4\pi \sin\theta/\lambda$, where 2θ is the scattering angle). To check for radiation damage, the data were collected in two 2-min exposures. These measurements indicated no changes in the scattering patterns with time, *i.e.* there was no measurable radiation damage. The data were averaged after normalization to the intensity of the incident beam, and the scattering of the buffer was subtracted. All data manipulations were performed using the program package PRIMUS (37).

The forward scattering $I(0)$ and the radius of gyration (R_g) were evaluated using the Guinier approximation assuming that, at very small angles ($s < 1.3/R_g$), the intensity is represented as $I(s) = I(0) \exp(-(sR_g)^2/3)$. These parameters and the maximum diameter (D_{max}) of the particle were also computed from the entire scattering patterns using the program GNOM (38). The excluded volume, V_p, of the particle was computed from the Porod invariant (39). The molecular masses of the solutes were evaluated by comparison of the forward scattering with that from reference solutions of bovine serum albumin (66 kDa).

The *ab initio* low resolution shape analysis of UL9ct was performed using the program DAMMIN (40). The program represents the molecule as a collection of $M \gg 1$ densely packed beads inside a sphere with D_{max}. Each bead belongs either to the molecule or to the solvent, and the shape is described by a binary string of length M. Starting from a random string, simulated annealing is employed to search for a compact model that fits the shape of the scattering curve $I(s)$ to minimize the discrepancy shown in Equation 2,

$$\chi^2 = \frac{1}{N-1}\sum_j \left(\frac{I(s_j) - cI_{calc}(s_j)}{\sigma(s_j)} \right)^2 \qquad \text{(Eq. 2)}$$

where N is the number of experimental points; c is a scale factor, and $I_{calc}(s_j)$ and $\sigma(s_j)$ are the calculated intensity and the experimental error at the momentum transfer s_j, respectively. The program GASBOR (41) was used to create *ab initio* models of the UL9ct protein consisting of dummy residues instead of beads. In this program a simulated annealing protocol is employed to construct a model with a protein-like distribution of beads that provides the best fit to the experimental data. For all *ab initio* analyses, multiple runs were performed to verify the stability and reliability of the solution.

The structure of the ICP8ΔC-UL9ct complex (with 1:1 stoichiometry) was refined by rigid body modeling using the program SASREF (42), which employs a simulated annealing protocol to generate an interconnected assembly of subunits without steric clashes fitting the scattering data. The monomer model of ICP8ΔC was taken from the crystal structure (27), whereas for UL9ct, the reconstructed *ab initio* envelope was used. The scattering amplitudes from the two proteins were calculated using the program CRYSOL (43). Two potential models were found by multiple runs of SASREF. Cross-linking results (see supplemental material) would marginally favor one of these models.

The *ab initio* model of the UL9ct-DNA complex was performed by a multiphase bead modeling program MONSA (44). This program describes the model by an assembly of beads inside a spherical search volume with the diameter equal to that of the complex. Simulated annealing is employed to find which bead belongs to which part of the complex (protein or DNA) by simultaneous fitting of two scattering curves (from the UL9ct-DNA complex and the theoretical dsDNA scattering alone). Several independent runs yielded reproducible models of UL9ct/DNA (with a 2:1 stoichiometry), which produced good fits to the experimental scattering profiles.

RESULTS

UL9ct Is a Monomeric Globular Protein

The experimental SAXS curves from the UL9ct protein are displayed in Fig. 1*A*, and the overall parameters computed from the data are presented in Table 1. The molecular mass of the UL9ct protein at the concentration 0.8 mg ml^{-1} is 38 ± 5 kDa, as estimated from the relative forward scattering intensity ($s = 0$), suggests that the protein is monomeric in solution, as expected at low concentration. This finding is further corroborated by the excluded (Porod) volume of the particle in solution of $(78 \pm 5) \times 10^3$ $Å^3$ using the empirical finding that for globular proteins the hydrated volume in $Å^3$ should numerically be about twice the molecular mass in daltons. The *ab initio* model for UL9ct as derived from an average of 10 GASBOR runs is

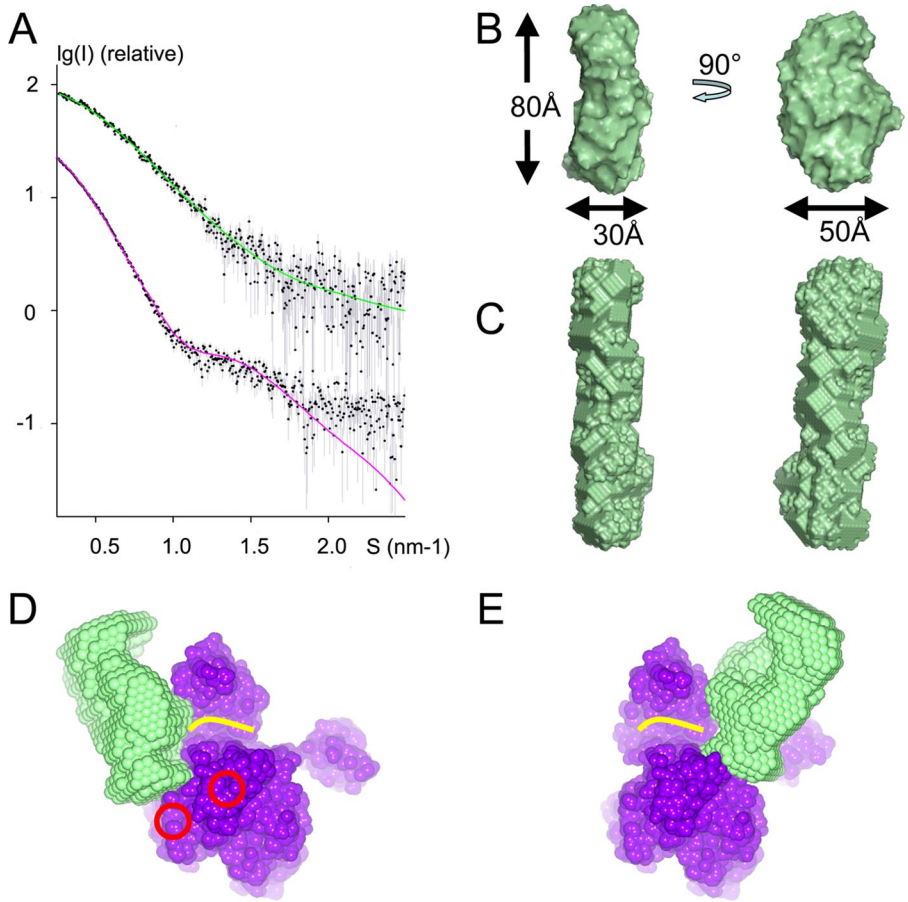

FIGURE 1. *A,* solution scattering curves (*dots* with *error bars*) for the UL9ct monomer (*lower*) and the UL9ct-ICP8ΔC complex (*upper*) together with the calculated curves for the models shown in *B* and *E*. *B,* molecular envelope of the UL9ct monomer as determined from solution scattering experiments with approximate dimensions. The two views are rotated with respect to each other by a 90° rotation about the vertical axis. *C,* envelope of the UL9ct dimer, which forms over time. *D* and *E,* two possible models of the UL9ct-ICP8ΔC binary complex derived from the x-ray scattering data using the known structure of ICP8ΔC and the envelope of UL9ct. The UL9ct envelope (*spheres* about the dummy residues) is shown in *green,* and a similar representation of ICP8ΔC is shown in *magenta*. The two ICP8ΔC domains (the smaller C-terminal helical domain (26) is seen as a protrusion on the *right*) were allowed to move independently in each case, constrained by a linker of 10 residues. The expected ssDNA-binding cleft (27) is indicated by a *yellow line,* indicating that ssDNA binding would be obstructed if UL9ct is bound. The *red circles* show the approximate positions of the surface lysines on ICP8ΔC that are modified by the cross-linker (supplemental material) suggesting a preference for the structure shown in *E*.

TABLE 1

Parameters of UL9ct and UL9ct-ICP8ΔC and UL9ct-DNA complexes calculated from the SAXS data

The abbreviations used are as follows: R_g, radius of gyration; D_{max}, maximum size of the particle; V_P, excluded volume of the hydrated particle, Experimental mass, experimental molecular mass of the solute.

Samples	Concentration	R_g	D_{max}	V_P	Experimental mass
	mg/ml	*nm*	*nm*	*nm*^{3}	*kDa*
UL9ct	0.8	2.63 ± 0.04	8.0 ± 0.5	78 ± 5	38 ± 5
UL9ct/ICP8ΔC	1.1	4.55 ± 0.06	16.0 ± 1.0	310 ± 10	140 ± 10
UL9ct/DNA	1.5	3.57 ± 0.05	12.5 ± 1.0	145 ± 10	78 ± 10

shown in Fig. 1*B*. The discrepancy factor for the fits, χ, was 1.65. It is apparent that after some hours UL9ct tends to irreversibly dimerize, and the *ab initio* envelope of the dimer restored by DAMMIN (χ = 1.97) is also shown in Fig. 1*C*. This time-dependent dimerization has required the use of freshly prepared protein and to consider the effects (especially at higher temperatures) of producing nonproductive material, with possible effects on the apparent stoichiometry.

UL9ct Forms a Stable 1:1 Complex with a 60-Amino Acid C-terminal Deletion of ICP8

High levels of UL9ct expression were attainable using the *E. coli* BL21(DE3)pLysS strain. ICP8ΔC was expressed in insect cells as an N-terminal His_6-tagged protein, which was then used to pull down UL9ct. The most efficient means of ICP8ΔC-UL9ct complex formation was by mixing the UL9ct cell lysate with the ICP8ΔC cell lysate and using the Äkta three-dimensional purification kit with a two-column strategy (nickel-chelating and size exclusion), as described under "Experimental Procedures."

The UL9ct-ICP8ΔC complex includes 354 + 1160 amino acids with an actual molecular mass of ~161 kDa. The complex eluted as a single peak with an apparent molecular size of ~170 kDa, based on the logarithm of molecular mass against protein standards that had been passed through the same column (data not shown). This finding suggested that the complex exists as a 1:1 heterodimer in solution, as reported previously. However, because the behavior of a protein during chromatography on a gel filtration column correlates directly with its Stokes radius and not always with its true molecular weight, other methods of determining the stoichiometry of the complex were also employed (see below).

At high concentrations (above 1.8 mg ml^{-1}) UL9ct starts to aggregate and precipitate, even at 4 °C. The addition of ICP8ΔC to UL9ct greatly stabilizes UL9ct even at higher concentrations (above 10 mg ml^{-1}), and no precipitation or degradation of the complex was observed.

For the SAXS model of the ICP8ΔC-UL9ct complex, the estimated molecular mass of the UL9ct-ICP8ΔC complex (at 1.1 mg ml^{-1}) is 140 ± 10 kDa, which is compatible with a 1:1 ratio for the complex. The excluded volume of the complex (310 ± 10) × 10^3 Å^3 is also in good agreement with 1:1 stoichiometry. Two potential models for the UL9ct-ICP8ΔC complex, as obtained using SASREF, and shown in Fig. 1, *D* and *E*, gave almost identical fits to the scattering data (χ = 1.41). Chemical cross-linking results (supplemental material) would slightly favor the model in Fig. 1*E*. The partial obstruction of the assumed (27) ssDNA-binding region of ICP8ΔC (in *yellow* in Fig. 1, *D* and *E*) by UL9ct is common to both models. This result implies that the complex will not bind to ssDNA, unless it first

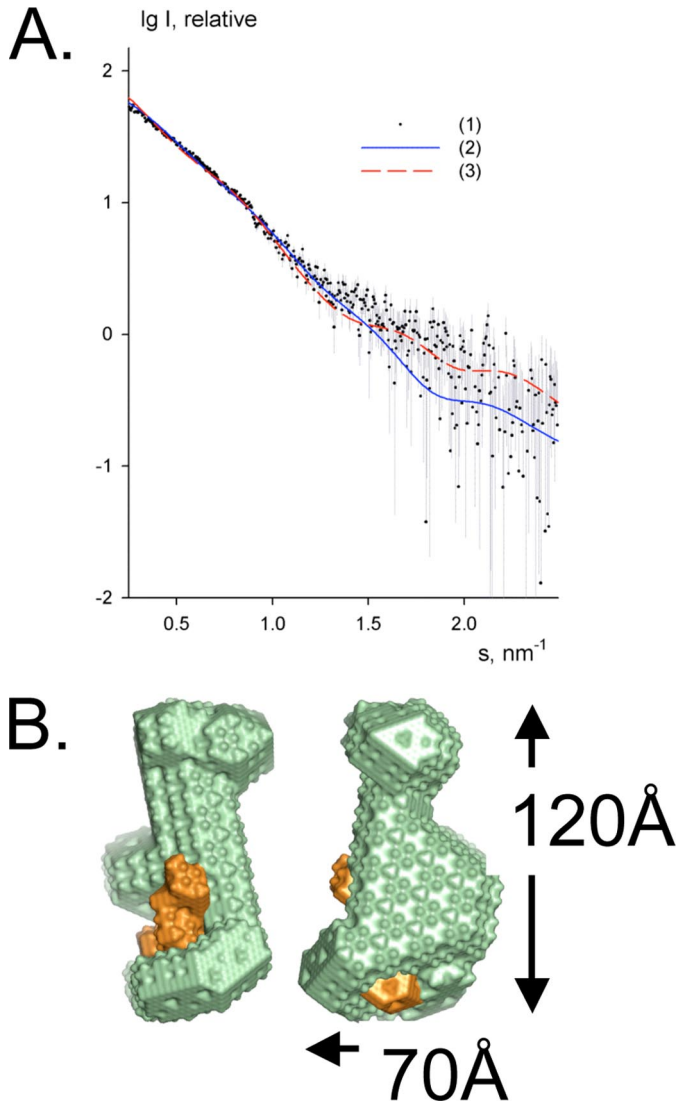

FIGURE 2. *A,* scattering curve for the UL9ct-dsDNA complex (*dots* with *errors bars*) with MONSA (*blue solid curve*) and SASREF fits (*red dashed curve*). *B, ab initio* MONSA envelope for the 2:1 UL9ct-dsDNA$_{15\text{-mer}}$ complex in two orientations related to each other by a vertical rotation of 90°. The protein is colored *green* and the DNA colored *brown*.

dissociates, whereupon ICP8ΔC alone will bind. We examined electron micrographs (supplemental material) of the UL9ct-ICP8ΔC complex incubated with ssDNA for times between 5 and 30 min. The micrographs showed longer continuous ICP8ΔC (only) covered tracts with time but were otherwise difficult to quantify.

At Micromolar Protein Concentrations, UL9ct and a dsDNA$_{15\text{-mer}}$ Containing the Box I Sequence Form a 2:1 Complex

SAXS Model of the UL9ct-DNA Complex—The analysis of the scattering curves (Fig. 2*A*) of the UL9ct-dsDNA$_{15\text{-mer}}$ complex (18 μM), using the program MONSA, which uses the experimental scattering curve of the complex together with the theoretical scattering for a 15-mer dsDNA, provides a low resolution structure of the complex (Fig. 2*B*) suggesting a 2:1 stoichiometry (the discrepancy factor for the fit $\chi = 1.58$). This is in agreement with the estimated excluded volume of UL9ct/dsDNA ($145 \pm 10 \times 10^3$ Å^3). The structure makes two important statements. First, the two UL9ct molecules in the complex are not identical in shape, and second, one UL9ct apparently either surrounds, or almost surrounds, the dsDNA. This agrees with previous work (19) based on cross-linking studies suggesting that the second UL9ct molecule does not contact the DNA. The 2:1 UL9ct-DNA complex is less extended than the dimer model of UL9ct (Fig. 1*C*).

Sedimentation Velocity of the UL9ct-DNA Complex—Although size exclusion chromatography is often used to estimate the molecular weights of proteins, the results can be misleading if the molecules are not entirely globular. A discrepancy is even more likely for DNA and protein-DNA complexes. In contrast, analytical ultracentrifugation is an absolute technique capable of directly measuring the sedimentation coefficient (s), diffusion coefficient (D), and the molecular mass of macromolecules, with no assumptions required as to their shape. Sedimentation velocity was therefore employed to examine the UL9ct-DNA complex. The experiment was performed at a 4:1 protein:DNA ratio (final DNA concentration of 2.4 μM). The absorbance was measured at 262 nm. The data were analyzed using the $c(s)$ program included in the UltraScan 7.1 software (Fig. 3). The results show that UL9ct forms a dimer when bound to its recognition sequence, because almost 80% of the species sediments at 2.80 S with an estimated molecular mass of ~79 kDa (compared with the predicted molecular mass of a 2:1 protein-DNA complex of 81 kDa). A smaller component (~14%) at 1.77 S is most probably free protein because its molecular mass is 37.8 kDa, which compares favorably with the theoretical value for a monomer (36 kDa), rather than that for a monomer protein-DNA complex (~45 kDa). Although there was a 2-fold excess of protein in this experiment, its absorption at 262 nm is very much less than that of DNA.

From these data, the frictional ratio of the free protein and the nucleoprotein complex can be obtained ($f/f_0 = 1.90$ and 2.17, respectively, after allowing for hydration). This indicates that UL9ct is a somewhat elongated protein, and the complex even more elongated, consistent with the SAXS results (Fig. 1*B* and Fig. 4*B*).

Isothermal Titration Calorimetric Analysis of the UL9ct Binding to Box I DNA—The exothermic reaction could be fitted (Fig. 4) by a two-step reaction, with thermodynamic parameters given in Table 2. In electrophoretic mobility shift assays, intermediate species were never observed. This may be explained if the second reaction has a lower K_d value than the first, which in turn implies that a (conformational) change occurs upon initial binding and that this enhances the affinity for the second binding event. Because the Box I DNA was injected into the UL9ct solution, it is expected for 2:1 UL9ct/DNA stoichiometry that the number of sites would be 0.5. The determined value of 0.33 implies either errors in the estimated concentrations of protein and DNA (which are not expected to be more than 10%) or a proportion of inactive UL9ct resulting from nonproductive dimerization at the temperature used, or both. We also investigated the binding of two UL9ct mutants, K746A and K758A, to the dsDNA$_{15\text{-mer}}$ by EMSA (supplemental material), which could also be analyzed in terms of a two-step model.

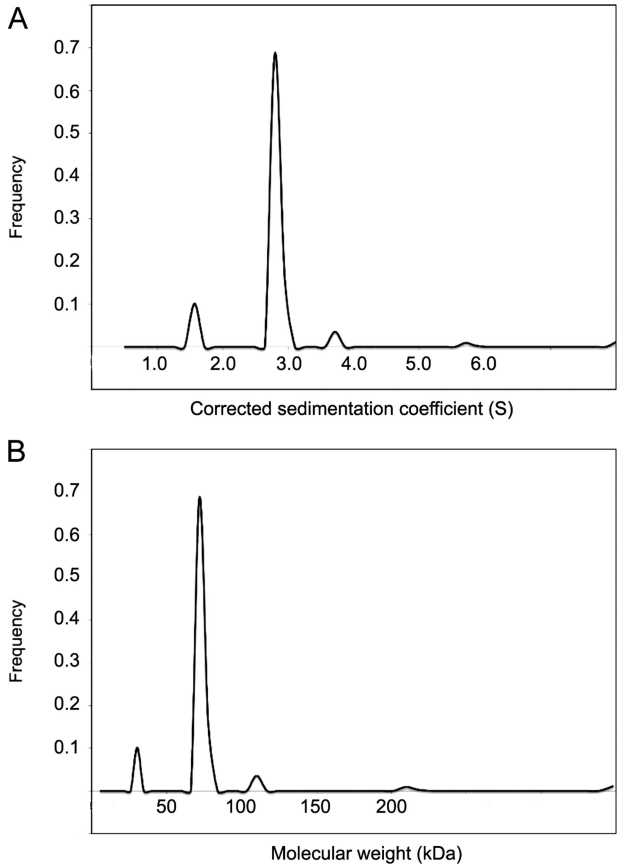

FIGURE 3. **Sedimentation velocity analysis.** *A*, distribution of sedimentation coefficients *c*(*s*). *B*, distribution of molecular weights *c*(M_r) for the 4:1 molar mixture of UL9ct and the dsDNA$_{15\text{-mer}}$. The analysis shows three species as follows: UL9ct (37.8 kDa, $s_{20,w}$ = 1.77 S, $D_{20,w} = 4.06 \times 10^{-7}$ cm^2 s^{-1}; % of mixture = 13.8), 2UL9ct:DNA (78.3 kDa, $s_{20,w}$ = 2.80 S. $D_{20,w} = 3.22 \times 10^{-7}$ cm^2 s^{-1}, % of mixture = 78.8)- and a higher molecular weight species (108.6 kDa; $s_{20,w}$ = 3.57S, $D_{20,w} = 2.85 \times 10^{-7}$ cm^2 s^{-1}, % of mixture = 7.4), which can be interpreted as a 3:1 UL9ct-DNA complex.

At Micromolar Protein Concentrations, UL9ct, ICP8ΔC, and the Box I-containing DNA Form a 2:1:1 Complex

Analytical Size Exclusion Chromatography of the Ternary Complex—The dsDNA$_{15\text{-mer}}$ used containing the Box I recognition sequence for UL9 located within the HSV-1 oriS was 5′-hexachlorofluorescein-labeled on the forward strand. The final concentration was 3 μM. During gel filtration chromatography, only the hexachlorofluorescein-labeled DNA was observed (540 nm). A 1:1:1 UL9ct:ICP8ΔC:dsDNA mixture was used, so as to observe whether the three macromolecules form a ternary complex in solution or not. Buffer GF (50 mM Tris-HCl, pH 8.0, 150 mM NaCl, and 5% (v/v) glycerol) was used with a Superose 6 HR 10/30 gel filtration column. No attempt was made, at least in part, to translate the elution volumes obtained from the two gel filtration runs to molecular mass because the presence of DNA would anyway tend to yield elongated rather than globular shapes. The only peak observed for the 1:1 ICP8ΔC:DNA mixture at 540 nm (Fig. 5*A*, *mauve curve*) corresponds to free DNA, and thus no ICP8ΔC-DNA complex is formed in solution, consistent with the EMSA result (see below). For the 1:1:1 UL9ct:ICP8ΔC:DNA mixture, three peaks were observed (Fig. 5*A*, *blue curve*). Subsequent 10% native PAGE analysis of the peak fractions suggested that the first peak

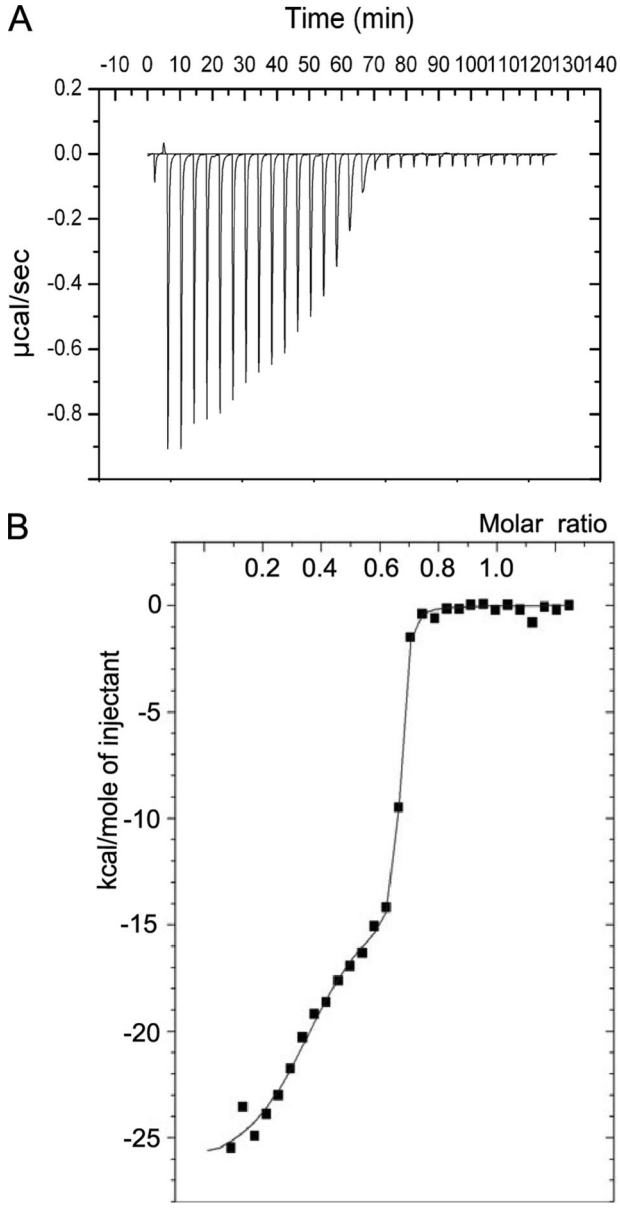

FIGURE 4. **Isothermal titration microcalorimetric analysis of the Box I-containing dsDNA$_{15\text{-mer}}$ to UL9ct.** *A*, trace of the calorimetric titration of 30 × 2.5-μl aliquots of 463 μM DNA injected into 1.8 ml of 15.8 μM UL9ct. *B*, *solid line* in the *lower plot* represents the best fit to the data given by the parameters in Table 2.

TABLE 2

Thermodynamic parameters for Box I dsDNA-UL9ct binding derived from the isothermal microcalorimetric titration

	First binding event	Second binding event
K_d (nM)	6.2 ± 2.5	0.81 ± 0.33
ΔH (kcal/mol)	−13.6 ± 1.1	−1.69 ± 1.0
ΔS (cal/mol/K)	−8	−48
No. of sites	0.32 ± 0.01	0.33 ± 0.01

corresponds to the ternary complex, the second peak corresponds to the UL9ct-DNA complex, and the third peak to free DNA (see the supplemental material). In a separate experiment, in a different buffer (Fig. 5*B*), the elution profiles monitored at 256 nm for free DNA (*green*), a 2:1 UL9ct:DNA mixture (*pink*) and a 1:1 UL9ct-DNA mixture (*blue*) confirm the 2:1 stoichiometry of the UL9ct-DNA complex.

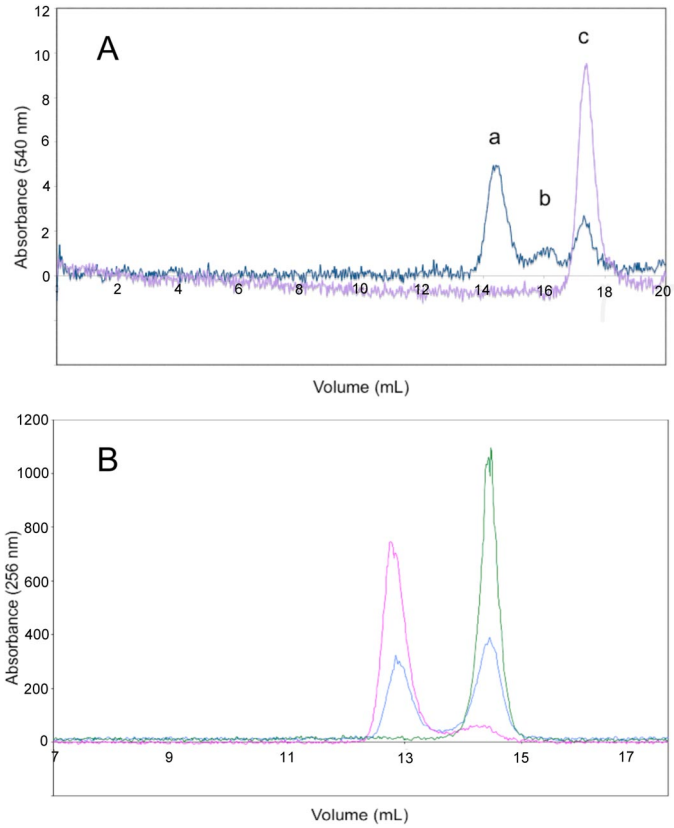

FIGURE 5. *A,* analytical gel filtration of the ternary complex using the fluorescein-labeled $dsDNA_{15\text{-}mer}$. The chromatogram in *mauve* is for a 1:1 ICP8ΔC:DNA mixture where only the DNA is observed, whereas the chromatogram in *blue* is for a 1:1:1 UL9ct:ICP8ΔC:DNA mixture. The labels are as follows: *a,* ternary ICP8ΔC-UL9ct-DNA complex; *b,* binary UL9ct-DNA complex; and *c,* free DNA. A native page of fractions *a–c* is given in the supplemental material. *B,* gel filtration of UL9ct:DNA mixtures at increasing protein concentration. Profiles shown are at protein:DNA ratios of 1:1 (*blue*) and 2:1 (*pink*) together with free DNA (*green*).

Gel Retardation Studies on the Binding of UL9ct and ICP8ΔC to a 15-mer dsDNA Template—The formation of the ternary complex was studied by EMSA, to elucidate the stoichiometric ratio of the interaction, again with proteins in the micromolar concentration range. Different combinations of UL9ct-ICP8ΔC-DNA were tested by 0.8% (w/v) agarose gel electrophoresis and are presented in Fig. 6. The gels were run for 60 min at 80 V and at 20 °C. The starting DNA concentration for all experiments was 3.33 μM. Based on the results presented in Fig. 6, the following conclusions can be drawn. ICP8ΔC does not interact with the dsDNA molecule used for these assays (Fig. 6, *A* and *B*, *lane 5*). UL9ct interacts with the particular dsDNA at the stoichiometric ratio of 2:1 (Fig. 6, *A* and *B*, *lanes 2–4,* and *C* and *D*, *lanes 2* and *3*). The UL9ct-ICP8ΔC-DNA complex (Fig. 6, *A* and *B*, *lanes 6–8,* and *C* and *D*, *lanes 4–6*) gives rise to a single band at the ratio of 2:1:1. Therefore, this ratio probably describes best the ternary complex interaction at these protein concentrations.

The ratio of shifted duplex DNA was measured by either a preincubation of UL9ct with the $dsDNA_{15\text{-}mer}$ and then addition of ICP8ΔC (Fig. 6, *A* and *B*), or with a preincubation of UL9ct with ICP8ΔC and then addition of $dsDNA_{15\text{-}mer}$ (Fig. 6, *C* and *D*). Upon preincubation of UL9ct with the duplex-DNA, the ternary complex formation may be less stable or less efficient (compare Fig. 6, *B*, *lane 7,* with *D*, *lane 5*).

Binding of UL9ct-ICP8ΔC Complexes to Herpes Simplex Virus Type 1 Origin Containing DNA (oriS)—The binding of the UL9ct-ICP8ΔC complex to oriS present on either super-twisted pGEM822 plasmid DNA or on the 822-bp HSV-1 BamHI fragment was examined by EM. The complexes were formed by incubating these DNAs with a 1:1 complex of UL9ct-ICP8ΔC for 1 h at 37 °C followed by preparation for EM. Examination of fields of DNA-protein complexes revealed that the binding of UL9ct/ICP8ΔC to dsDNA is highly efficient. With the super-twisted template (Fig. 7, *A* and *B*), 43% ($n = 121$) of the DNA had no protein bound, 57% showed one complex, and no DNAs were observed with two or more complexes bound, arguing for a very low level of nonspecific binding. This is a significantly higher specificity (>50%) than in previous studies (16) where the full-length UL9 and ICP8 proteins were incubated with the same DNA template. There, a background of nonspecific binding was observed, possibly due to the binding of the full-length proteins to sites on the super-twisted DNA-containing single-stranded character.

To further illustrate the specific binding of UL9ct/ICP8ΔC to oriS, the 822-bp fragment in which oriS is located one-third the distance from the nearest end was incubated with UL9ct/ICP8ΔC and prepared for EM. Examination of fields of these complexes (Fig. 7, *C* and *D*) revealed that 22% ($n = 137$) of the DNAs were bound by a single large protein complex at a site one-third the distance from one end, and only 3% showed protein bound at sites not consistent with oriS. The remaining 75% of the DNA appeared protein-free. When super-twisted or linear DNAs lacking oriS were incubated with UL9ct/ICP8ΔC in parallel with the experiments above, less than 4% ($n = 124$ and 156, respectively) of the DNAs showed any large protein complexes bound. The complexes bound to both the super-twisted and linear templates were homogeneous in size and shape suggesting that evaluation of their mass would prove useful.

The mass of the protein complexes bound at oriS was evaluated using internal mass standards as described previously (37). Apoferritin, which is roughly spherical in shape and has a mass of 443 kDa, was selected as a mass standard. For these measurements, complexes of UL9ct-ICP8ΔC were formed on the 822-bp oriS fragment; the complexes fixed in place, and then just prior to mounting for EM, apoferritin was added. The projected areas of the protein complexes on the DNA and apoferritin molecules were determined from the micrographs allowing an estimate of the mass of the DNA-protein complexes to be made. This analysis revealed that the average calculated volume of the UL9ct-ICP8ΔC complex bound to oriS exceeded an average volume of apoferritin by 1.78-fold. Thus, the molecular mass of the UL9ct-ICP8ΔC complexes bound to oriS is estimated to be 790 ± 211 kDa ($n = 24$). The projected areas of the apoferritin particles varied only by 10% ($n = 12$) suggesting that the UL9ct-ICP8ΔC complex is more heterogeneous in size than the internal marker. The combined mass of a 2:1 UL9ct/ICP8ΔC is ~197 kDa, suggesting that around four copies (average 4.1 ± 1.0) are bound at oriS. This suggestion is speculative for two reasons. First, the EM images were recorded at protein concentrations 2 orders of magnitude lower than the *in vitro*

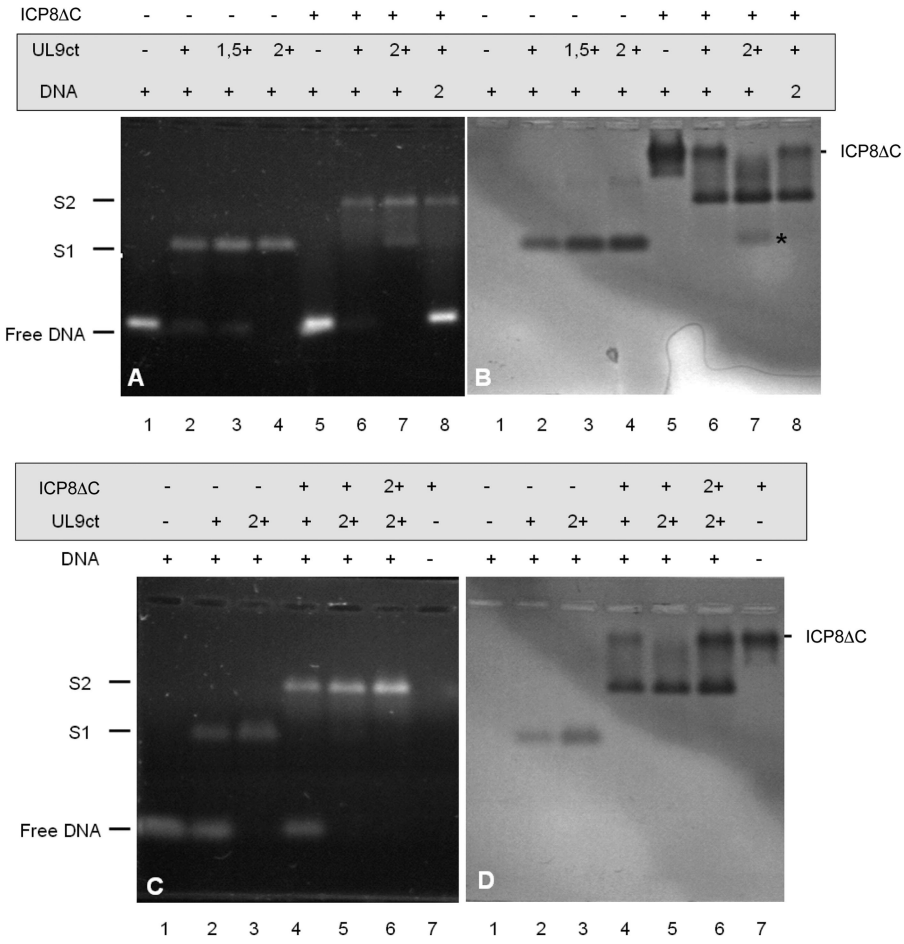

FIGURE 6. **Binding of UL9ct and UL9ct-ICP8ΔC complex to dsDNA$_{15\text{-mer}}$ was analyzed using agarose gel electrophoresis (1% TBE).** We measured the ratio of shifted duplex DNA by either a preincubation of UL9ct with the duplex DNA (*A* and *B*) and then addition of ICP8ΔC, or with a preincubation of UL9ct with ICP8ΔC (*C* and *D*) and then addition of duplex DNA. *A* and *C* show ethidium bromide-stained gels, and *B* and *D* show the Coomassie staining of the same gels. *S1* corresponds to the binary UL9ct-DNA complex, and *S2* corresponds to the ternary ICP8ΔC-UL9ct-DNA complex. + denotes the presence of one of the components, and − denotes its absence. *1.5* and *2* indicate the molar ratios of these components in the mixture. Where a number is absent the molar ratio is unity. *Asterisk* shows "free" pre-formed 2:1 UL9ct-DNA complex that is not bound to ICP8ΔC.

assays, and consequently the ratio of 1:1 and 2:1 UL9ct-DNA complexes will differ. Second, an extrapolation of our results on Box I binding to that on the full oriS is simplistic, in that it does not address rearrangements in oriS.

DISCUSSION

UL9ct was expressed and purified in high yields, and it was possible to concentrate the pure protein, without aggregation, to a concentration of 1.8 mg ml^{-1} (50 μM). At higher concentrations the protein starts to aggregate and upon prolonged storage at 4 °C even to precipitate. The initial process is via dimer formation and a possible physiological importance of this is discussed below, even though the dimerization of the full-length protein (UL9) is driven by the N-terminal domain, which is missing in our construct. The importance of a possible pseudo-leucine zipper (aa 570–591), which could result in dimerization (45), is less certain. A consequence, however, is that UL9ct is a difficult target for crystallization, compounded by a conformational flexibility suggested by the results presented in this paper, and we have had no success in extensive crystallization trials. Consequently, we decided to investigate the low resolution structure from freshly prepared samples using SAXS. SAXS measurements were performed successfully at concentrations of 0.8 mg ml^{-1} for UL9ct alone, and at 1.5 mg ml^{-1} for the complex with a dsDNA$_{15\text{-mer}}$ containing the Box I consensus sequence. The molecular mass of UL9ct, estimated from the relative forward scattering intensity, was 38 ± 5 kDa, suggesting that the protein is monomeric in solution at low concentration. The low resolution shape of UL9ct was reconstructed *ab initio* using the programs DAMMIN and GASBOR. The average of 10 runs of the latter is shown in Fig. 1*B*. Over a period of time it seems that UL9ct dimerizes, but this dimer is more elongated than that observed in the UL9ct-DNA complex (compare Fig. 1*C* and Fig. 4*B*).

Although UL9ct exists as a monomer in solution at low concentrations, there has been some discussion as to whether one (22–24) or two (25, 26) molecules bind to a single Box I recognition sequence. In this work, by using a variety of biophysical techniques, we show that it forms a UL9ct-dsDNA 2:1 complex at micromolar protein concentrations, although the K_d value derived from the ITC experiments suggests that a 1:1 complex will predominate at sub-nanomolar concentrations, consistent with previous work (22). As mentioned above, UL9ct is monomeric in solution, but we do observe, in the absence of ICP8ΔC, a tendency to dimerize. Furthermore, the EMSA and analytical ultracentrifugation experiments on the UL9ct/dsDNA show evidence for the formation of higher molecular weight species, which could be interpreted as a 3:1 complex, indicative of further UL9ct-UL9ct interactions. Whether these interactions are specific or not and whether the resulting complexes are nonproductive are harder to establish.

ICP8 binds to the extreme C terminus of the full-length UL9 protein and enhances both its helicase and DNA-dependent ATPase activities (8, 12, 13, 16, 19, 46). Although the mechanism by which it does so has not been elucidated, removal of the C-terminal 27 aa of the UL9 protein results in loss of the ability to bind ICP8 and enhanced ability of UL9 to unwind dsDNA *in vitro* (8, 11, 47). Thus, the C-terminal part of UL9 has been suggested to negatively regulate the activity of UL9, and binding of ICP8 to this region is proposed to abolish that regulation by masking that domain and/or by altering the conformation of the protein (19, 47,

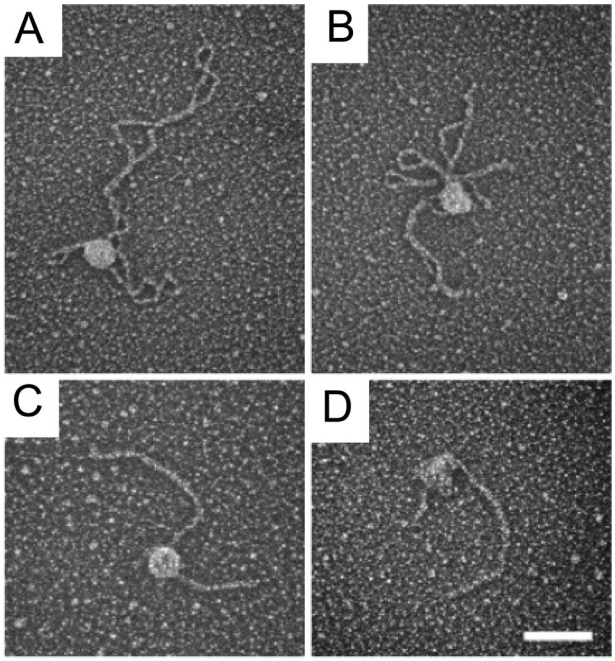

FIGURE 7. **ICP8ΔC/UL9ct binding to dsDNA containing the full HSV-1 replication origin (oriS).** ICP8ΔC-UL9ct complex was incubated with either a super-twisted plasmid pGEM822 (*A* and *B*) or BamHI fragment (822 bp) purified from pGEM822 plasmid containing HSV-1 oriS and prepared for EM analysis as described under "Experimental Procedures" (*C* and *D*). The *scale bar* represents 100 nm.

48). It has been previously reported (13, 23) that UL9ct and full-length ICP8 form a complex with a 1:1 stoichiometry. In this study we have shown that a 60-aa C-terminal deletion of ICP8 (which makes the protein less liable to aggregation) also binds very efficiently to UL9ct, suggesting that the missing part of ICP8 does not play any important role in the interaction of these proteins.

We have determined the low resolution model of an ICP8ΔC-UL9ct (1:1) complex. Fig. 1, *D* and *E*, shows two models obtained by analysis of the small angle scattering data, using the (known) crystal structure of ICP8ΔC and the scattering data from UL9ct alone and in complex with ICP8ΔC. Because we cannot distinguish between these models with the SAXS data alone, we performed cross-linking assays, and although we were unable to identify any intermolecular cross-linked residues the work (described in detail in the supplementary material) suggests a preference for the SAXS model in Fig. 1*E*.

For binding of UL9ct/ICP8ΔC to oriS, the interaction between ICP8 and UL9 is known to depend upon the nature of the DNA (ss or ds). For example, an ssDNA-oligo$(dT)_{65}$ completely prevents full-length ICP8 from binding to a complex between UL9ct and oriS (23). This may indicate a preference for ICP8 to bind to ssDNA or that the ssDNA-binding region of full-length ICP8 competes with the UL9ct-binding region or that the ICP8 changes its conformation substantially on binding to ssDNA such that it is no longer able to bind UL9ct. Our data support a model whereby an ICP8ΔC-UL9ct complex increases the ability to bind to another UL9ct molecule already bound to oriS. It is clear that if two UL9ct molecules bind to Box I of the origin, they must have different conformations, because Box I is not a palindrome sequence. We suggest that by binding to Box I UL9ct undergoes a conformational change that enhances its affinity for binding to another UL9ct molecule, perhaps already in complex with ICP8. This hypothesis is consistent with the fact that the EMSA, gel filtration, and analytical ultracentrifugation results demonstrate a 2:1 UL9ct:DNA stoichiometry at micromolar protein concentrations. The ITC studies, however, show the existence of a two-step reaction. We show that the dimeric species we observe after letting UL9ct age is different (Fig. 2*B versus* Fig. 1*C*) from the UL9ct dimer bound to Box I, further suggesting that binding of UL9ct to Box I accelerates a conformational change, different from nonproductive dimer formation, which is necessary to form a UL9ct-UL9ct interaction. Given the measured K_d value, appreciable concentrations of a 1:1 complex are expected in equilibrium conditions at nanomolar concentrations and below (22). It is difficult to extrapolate this to a cellular context because not only are the cellular concentrations of UL9 rather uncertain, but given the localization of the replisome to promyelocytic leukemia-containing regions (49), it is far from certain that *in vitro* equilibrium studies can describe the local environment.

In this study we have chosen to use truncated proteins in combination with a minimal dsDNA recognition sequence to have experimentally pure and tractable material. It is therefore essential to establish whether or not these truncated proteins assemble on oriS in the same way as the unmodified replication complex. In a previous study (16) of the binding of full-length UL9 and ICP8 to oriS, using the same templates used in this work, similar levels of binding were observed for super-twisted DNA. 58% of the super-twisted DNA contained one complex *versus* 57% in this study. However in the earlier study approximately one-third of the complexes on super-twisted DNA were not localized to oriS. In this study the very low level of binding to super-coiled DNA lacking oriS (4%) suggests that the level of nonspecific binding was much lower. The suggestion that the ICP8ΔC-UL9ct complex has a higher specificity of binding was reflected in the fact that previously only 14% of the linear fragments containing oriS showed a protein complex assembled at oriS in contrast to >22% in this study.

It is established from biochemical studies that the minimal origin complex consists of two UL9 protein dimers bound at oriS (4, 25, 50, 51). This conclusion was verified in subsequent EM studies where these origin complexes have been directly visualized (16, 52). In the previous EM studies when full-length UL9 and ICP8 proteins were assembled at oriS (16), the size of the complex suggested that four copies of UL9 and two copies of ICP8 assemble at oriS. However, with the full-length proteins there was a large variation in the size of the bound complex, and in addition, the efficiency of binding to linear dsDNA was not high. Here, using the truncated forms of both proteins, we have found that the assembly of the UL9-ICP8 co-complex is more efficient, and hence we infer tighter binding. In addition a more uniform distribution of particle sizes at oriS was observed. This has made it possible to carry out a more precise EM-based mass analysis measurement than was possible in the previous work. The result of our mass analysis of the UL9ct-ICP8ΔC complex at oriS suggested that there are 3–4 copies of a 2:1 UL9ct-ICP8ΔC complex, assuming that the binding to a single Box I sequence involves two molecules of UL9ct and one of ICP8ΔC. This would fit well with the previous work showing that two

UL9 dimers are present at oriS in the absence of ICP8, if each molecule of the conformationally altered UL9 monomer was able to recruit a UL9-ICP8 complex to the origin.

On the basis of our results, we suggest that the binding of a UL9 molecule to the recognition sequence induces a conformational change in the C-terminal domain of UL9, which enhances the recruitment of a second UL9 molecule via an interaction between C-terminal domains. We thank a referee for pointing out that this conformational change must also result in the C-terminal tail of the UL9 molecule, that it is not interacting with ICP8, thus becoming inaccessible. Given the affinity of UL9 for ICP8 (also for the truncated proteins used in this study), this would be a mechanism for recruiting ICP8 to the origin of replication. Such recruitment is necessary because ICP8 itself does not have affinity for dsDNA but only for ssDNA or ssDNA overhangs of duplex DNA. The N-terminal ATP-dependent helicase function of UL9 can then open the origin, allowing ICP8 to bind to ssDNA and start its own ATP-independent, dsDNA unwinding activity. Recruitment of ICP8 is probably also important for recruiting the rest of the replication complex. Finally, we note that our work principally concerns the proteins bound to duplex Box I and pays scant attention to the rearrangement of oriS and the possible binding of UL9 to a DNA hairpin formed from Box I and Box III, which is reported (3, 17) to form upon activation of the origin, oriS.

Acknowledgments—We thank the staff of EMBL-SAXS group for support and for access to the X33 beamline and Borries Demeler for invaluable advice on the interpretation of the analytical ultracentrifugation measurements. We thank Luminita Damian for help in ITC data analysis and interpretation. Electron microscopic work was supported by National Institutes of Health Grants GM31819 and CA19014 to J. D. Griffith, Lineberger Comprehensive Cancer Center, University of North Carolina, Chapel Hill.

REFERENCES

1. Boehmer, P. E., and Lehman, I. R. (1997) *Annu. Rev. Biochem.* **66,** 347–384
2. Aslani, A., Macao, B., Simonsson, S., and Elias, P. (2001) *Proc. Natl. Acad. Sci. U. S. A.* **98,** 7194–7199
3. Macao, B., Olsson, M., and Elias, P. (2004) *J. Biol. Chem.* **279,** 29211–29217
4. Weir, H. M., and Stow, N. D. (1990) *J. Gen. Virol.* **71,** 1379–1385
5. Gustafsson, C. M., Hammarsten, O., Falkenberg, M., and Elias, P. (1994) *Proc. Natl. Acad. Sci. U. S. A.* **91,** 4629–4633
6. Hammarsten, O., and Elias, P. (1997) *Nucleic Acids Res.* **25,** 1753–1760
7. Makhov, A. M., Boehmer, P. E., Lehman, I. R., and Griffith, J. D. (1996) *EMBO J.* **15,** 1742–1750
8. Boehmer, P. E., Craigie, M. C., Stow, N. D., and Lehman, I. R. (1994) *J. Biol. Chem.* **269,** 29329–29334
9. McLean, G. W., Abbotts, A. P., Parry, M. E., Marsden, H. S., and Stow, N. D. (1994) *J. Gen. Virol.* **75,** 2699–2706
10. Monahan, S. J., Grinstead, L. A., Olivieri, W., and Parris, D. S. (1998) *Virology* **241,** 122–130
11. Boehmer, P. E. (1998) *J. Biol. Chem.* **273,** 2676–2683
12. Boehmer, P. E., Dodson, M. S., and Lehman, I. R. (1993) *J. Biol. Chem.* **268,** 1220–1225
13. Boehmer, P. E., and Lehman, I. R. (1993) *Proc. Natl. Acad. Sci. U. S. A.* **90,** 8444–8448
14. Lee, S. S., and Lehman, I. R. (1997) *Proc. Natl. Acad. Sci. U. S. A.* **94,** 2838–2842
15. He, X., and Lehman, I. R. (2001) *Proc. Natl. Acad. Sci. U. S. A.* **98,** 3024–3028
16. Makhov, A. M., Lee, S. S., Lehman, I. R., and Griffith, J. D. (2003) *Proc. Natl. Acad. Sci. U. S. A.* **100,** 898–903
17. Aslani, A., Simonsson, S., and Elias, P. (2000) *J. Biol. Chem.* **275,** 5880–5887
18. Aslani, A., Olsson, M., and Elias, P. (2002) *J. Biol. Chem.* **277,** 41204–41212
19. Lee, S. S., and Lehman, I. R. (1999) *J. Biol. Chem.* **274,** 18613–18617
20. Weir, H. M., Calder, J. M., and Stow, N. D. (1989) *Nucleic Acids Res.* **17,** 1409–1425
21. Hazuda, D. J., Perry, H. C., Naylor, A. M., and McClements, W. L. (1991) *J. Biol. Chem.* **266,** 24621–24626
22. Simonsson, S., Samuelsson, T., and Elias, P. (1998) *J. Biol. Chem.* **273,** 24633–24639
23. Gustafsson, C. M., Falkenberg, M., Simonsson, S., Valadi, H., and Elias, P. (1995) *J. Biol. Chem.* **270,** 19028–19034
24. Martin, D. W., and Deb, S. (1994) *J. Virol.* **68,** 3674–3681
25. Fierer, D. S., and Challberg, M. D. (1995) *J. Biol. Chem.* **270,** 7330–7334
26. Stabell, E. C., and Olivo, P. D. (1993) *Nucleic Acids Res.* **21,** 5203–5211
27. Mapelli, M., Panjikar, S., and Tucker, P. A. (2005) *J. Biol. Chem.* **280,** 2990–2997
28. Lee, C. K., and Knipe, D. M. (1985) *J. Virol.* **54,** 731–738
29. Stow, N. D., Brown, G., Cross, A. M., and Abbotts, A. P. (1998) *Virology* **240,** 183–192
30. Laue, T. M., Shah, B. D., Ridgeway, T. M., and Pelletier, S. L. (1992) in *Analytical Ultracentrifugation in Biochemistry and Polymer Science* (Harding, S. E., Rowe, A. J., and Horton, J. C., eds) pp. 90–125, Royal Society of Chemistry, Cambridge, UK
31. Durchschlag, H. (1986) in *Thermodynamic Data for Biochemistry and Biotechnology* (Hinz, H.-J., ed) pp. 80–81, Springer-Verlag, New York
32. Rasimas, J. J., Pegg, A. E., and Fried, M. G. (2003) *J. Biol. Chem.* **278,** 7973–7980
33. Wong, S. C., and Schaffer, P. A. (1991) *J. Virol.* **65,** 2601–2611
34. Griffith, J. D., and Christiansen, G. (1978) *Annu. Rev. Biophys. Bioeng.* **7,** 19–35
35. Griffith, J. D., Makhov, A., Zawel, L., and Reinberg, D. (1995) *J. Mol. Biol.* **246,** 576–584
36. Roessle, M. W., Klaering, R., Ristau, U., Robrahn, B., Jahn, D., Gehrmann, T., Konarev, P., Round, A., Fiedler, S., Hermes, C., and Svergun, D. (2007) *J. Appl. Crystallogr.* **40,** S190–S194
37. Konarev, P. V., Volkov, V. V., Sokolova, A. V., Koch, M. H. J., and Svergun, D. I. (2003) *J. Appl. Crystallogr.* **36,** 1277–1282
38. Svergun, D. I. (1992) *J. Appl. Crystallogr.* **25,** 495–503
39. Porod, G. (1982) in *General Theory, in Small-angle X-ray Scattering* (Glatter, O., and Kratky, O., eds) pp. 17–51, Academic Press, London
40. Svergun, D. I. (1999) *Biophys. J.* **76,** 2879–2886
41. Svergun, D. I., Petoukhov, M. V., and Koch, M. H. J. (2001) *Biophys. J.* **80,** 2946–2953
42. Petoukhov, M. V., and Svergun, D. I. (2005) *Biophys. J.* **89,** 1237–1250
43. Svergun, D. I., Barberato, C., and Koch, M. H. J. (1995) *J. Appl. Crystallogr.* **28,** 768–773
44. Svergun, D. I., and Nierhaus, K. H. (2000) *J. Biol. Chem.* **275,** 14432–14439
45. Deb, S., and Deb, S. P. (1991) *J. Virol.* **65,** 2829–2838
46. Dodson, M. S., and Lehman, I. R. (1993) *J. Biol. Chem.* **268,** 1213–1219
47. Murata, L. B., and Dodson, M. S. (1999) *J. Biol. Chem.* **274,** 37079–37086
48. Arana, M. E., Haq, B., Tanguy Le Gac, N., and Boehmer, P. E. (2001) *J. Biol. Chem.* **276,** 6840–6845
49. Burkham, J., Coen, D. M., and Weller, S. K. (1998) *J. Virol.* **72,** 10100–10107
50. Koff, A., Schwedes, J. F., and Tegtmeyer, P. (1991) *J. Virol.* **65,** 3284–3292
51. Elias, P., Gustafsson, C. M., Hammarsten, O., and Stow, N. D. (1992) *J. Biol. Chem.* **267,** 17424–17429
52. Makhov, A. M., Boehmer, P. E., Lehman, I. R., and Griffith, J. D. (1996) *J. Mol. Biol.* **258,** 789–799

Structural and Biophysical Characterization of the Proteins Interacting with the Herpes Simplex Virus 1 Origin of Replication

Ioannis Manolaridis, Eleni Mumtsidu, Peter Konarev, Alexander M. Makhov, Stephen W. Fullerton, Andrea Sinz, Stefan Kalkhof, John E. McGeehan, Peter D. Cary, Jack D. Griffith, Dmitri Svergun, Geoff G. Kneale and Paul A. Tucker

J. Biol. Chem. 2009, 284:16343-16353.
doi: 10.1074/jbc.M806134200 originally published online March 27, 2009
